Polymer Light-Emitting Electrochemical Cells: A Theoretical Study of Junction Formation under Steady-State Conditions

José A. Manzanares and Howard Reiss

Department of Chemistry and Biochemistry, University of California at Los Angeles, Los Angeles, California 90024

Alan J. Heeger

Institute for Polymers and Organic Solids, University of California at Santa Barbara, Santa Barbara, California 93106

The Journal of Physical Chemistry B®

Reprinted from
Volume 102, Number 22, Pages 4327–4336

Polymer Light-Emitting Electrochemical Cells: A Theoretical Study of Junction Formation under Steady-State Conditions

José A. Manzanares and Howard Reiss*

Department of Chemistry and Biochemistry, University of California at Los Angeles, Los Angeles, California 90024

Alan J. Heeger

Institute for Polymers and Organic Solids, University of California at Santa Barbara, Santa Barbara, California 93106

Received: October 21, 1997; In Final Form: March 24, 1998

The performance of light-emitting electrochemical cells is studied under steady-state conditions. The theoretical model presented is based on the approach to electrodiffusion−reaction problems familiar with electrochemical cells. However, some links with the traditional semicondutor physics approach are also presented. The reversible redox electrode reactions are considered to always be in thermodynamic equilibrium, and the distribution of the applied potential between the two electrode/polymer interfaces and the active layer is carefully analyzed by the numerical solution of the transport equations. The theory is able to explain most of the experimental observations. In particular, the junction formation is proved to be a bulk process related to the electrodiffusion and recombination reaction of polarons, thus explaining its macroscopic nature. Current−voltage and light−voltage characteristics in qualitative agreement with experiment are found. The observed changes in the junction width and the electric field profile with applied voltage are also accounted for. Some ideas for future work are also discussed.

1. Introduction

The electrochemistry of π-conjugated polymers such as poly-(1,4-phenylenevinylene) (PPV) involving the reversible doping of a polymer backbone to form n-type or p-type materials and their application to display technology has become an attractive field, especially because of the successful use of these active materials in polymer-based photoconductive and light-emitting diodes (LEDs)[1−3] as well as polymer light-emitting electrochemical cells (LECs).[4−9]

The active layer in these LECs is a polymer blend with a phase-separated bicontinuous network morphology[5] which combines the electrochemical properties of conjugated polymer with the ionic conductivity of polymer electrolyte.[10] This blend can be either sandwiched between two contact electrodes (Al and indium-tin oxide, ITO) or spin-cast onto a glass substrate with parallel, interdigitated gold electrodes in a surface cell configuration. Following previous work with cross-linked polyethers containing dissolved alkali-metal salts and electroactive solutes,[11] LEC devices have often been fabricated with PPV or poly[2-methoxy-5-(2′-ethylhexyloxy)-1,4-phenylenevinylene] (MEH-PPV) admixed with a complex of poly(ethylene oxide) (PEO) and lithium trifluoromethanesulfonate.[4−9]

Electrochemical doping is initiated when the applied voltage is greater than E_g, the energy gap of the semiconductor polymer, which has been determined as 2.4 eV for PPV and 2.1 eV for MEH-PPV.[8] The luminescent polymer adjacent to the anode becomes p-type doped, while the polymer adjacent to the cathode becomes n-type doped. This doping process is accompanied by a redistribution of the ions from the polymer electrolyte which moves to preserve local electroneutrality. The injected electrons and holes flow toward the center of the active layer, where they recombine and decay radiatively. To optimize the LEC performance, it then becomes necessary to understand the processes that control charge recombination.[3]

The nature of this electrochemically induced p−n junction has been recently studied by the optical beam induced current method (OBIC).[9] However, the width and shape (i.e., the doping profile) of the junction are not yet understood in detail. Previous studies on this subject have described the p−n junction in a LEC following a semiconductor physics approach. Based on optical microphotographs of the working LEC[4,7] and the OBIC scans,[9] these studies have implicitly assumed that approximately homogeneous p-type and n-type doping is achieved up to the inner region of the LEC, so that a well-defined p−n junction is formed. Consistent with this view, it has been assumed that any applied bias potential adds primarily across this junction. Therefore, the minimum bias necessary to maintain the p−n junction equals the LUMO−HOMO band gap of the luminescent polymer divided by the elementary charge E_g/e, and any further increase in the bias voltage leads to the flow of electrons and holes into the junction, resulting in recombination and light emission.

However, the semiconductor physics approach cannot explain why the junction width is observed to be a function of the interelectrode spacing (or cell thickness) and, more important, why the junction is so thick. In particular, in a sandwich cell configuration, the junction width was estimated to be 0.15 and 2 μm for anode-to-cathode spacings of 0.30 and 15 μm, respectively. In planar cell configurations, the junction width was estimated as 1 and 2.5 μm for 10 and 30 μm interelectrode spacing, respectively.[6] Furthermore, the OBIC scans[9] show that the electric field profile due to the junction extends over a region

S1089-5647(97)03415-9 CCC: $15.00
Published on Web 05/07/1998

on the order of a few micrometers and that the maximum electric field goes to zero when the bias voltage is close to the $\pi-\pi^*$ energy gap. A typical semiconductor junction, however, would exhibit a large electric field (extending over a region of tenths or hundredths of a micrometer) under these conditions.

These previous studies of the p−n junction in LECs seem to have neglected the fact that the mobility of the ions in the polymer electrolyte may have an important influence on the nature of the junction. In the same way that graded p−n junctions or even p−i−n junctions appear in semiconductor devices where the donor- or acceptor-type defects are mobile,[12] the junction in LECs could also consist of either a graded junction (with the graded doping profile extending over most of the cell) or two doped layers separated by an inner region depleted of ions, in the case that the salt concentration in the polymer electrolyte is not sufficiently high. Also, recent electroluminescence studies of bilayer LEDs confirm that the spatial extent of the active zone is limited by the recombination of charge carriers injected at the electrode contacts,[3] i.e., electroluminescence in LEDs is essentially a bulk phenomenon with a spatial extent controlled by the mobility of the charge carriers and the recombination rate.

In this paper we address the problem of junction formation and recombination in LECs. Our main goal is to provide theoretical insight into the basic phenomena by adopting the approach to electrodiffusion−reaction problems commonly used in the treatment of electrochemical cells. In particular, the distribution of the applied potential between the two electrode/polymer interfaces and inside the active layer (i.e., the potential difference between the n- and p-type layers) is studied. The reversible redox electrode reactions are assumed to achieve instantaneous thermodynamic equilibrium.[13,14] The steady-state transport equations for the charged polaronic species are solved within the active layer, where the recombination of oppositely charged polaronic species takes place. In addition, the electrodes are considered to be inert, so that the ionic contribution to the current is zero under steady-state conditions.[4] This model, although simple, describes the observed current−voltage and light−voltage characteristics of LECs,[4−7] while providing a clear understanding of the doping profile and junction width as a function of bias potential. The macroscopic nature of the junction (as a result of the electrodiffusion−reaction process) and its dependence on the interelectrode spacing is also clarified.

2. Theory

The blend of semiconducting polymer and polymer electrolyte is modeled as a one-dimensional homogeneous system where all parameters depend only on position coordinate x ($0 < x < L$, L being the distance between the electrodes). The semiconducting polymer is described as a continuum of conjugated chain segments that may remain unoccupied (P^0) or contain at most one charged polaron (either P^- or P^+).[10,14,15] The concentration of conjugated chain segments will be denoted by c_m, the concentrations of charged polarons by c_{P^-} and c_{P^+}, and that of unoccupied chain segments by $c_{P^0} = c_m - c_{P^-} - c_{P^+}$; all of them are given in cm^{-3} units. The polymer electrolyte is described as a strong electrolyte solution that coexists with the semiconducting polymer. The particle concentrations of ion species are denoted by c_{A^-} and c_{C^+}.

(a) Thermodynamic Equilibrium at the Electrode/Polymer Interfaces. Since the electrodes are inert to the polymer electrolyte and the conjugated chain segments may accommodate excitations of either charge type, the following two electrode reactions may take place at the electrode/polymer interfaces

$$P^0 + e^- \rightleftarrows P^- \tag{1a}$$

$$P^0 \rightleftarrows P^+ + e^- \tag{1b}$$

These electrode reactions are considered to be in instantaneous local equilibrium (i.e., the electrode kinetics is fast compared to the charge transport),[13,14] so that the Galvani potential differences between the metal and the adjacent polymer, $\Delta_m^p\phi \equiv \phi^p - \phi^m$, are given by the Nernst equations

$$\Delta_m^p\phi = \Delta\phi_{P^-}^0 + \frac{kT}{e}\ln\frac{c_{P^-}}{c_{P0}} \tag{2a}$$

$$\Delta_m^p\phi = \Delta\phi_{P^+}^0 - \frac{kT}{e}\ln\frac{c_{P^+}}{c_{P0}} \tag{2b}$$

where $\Delta\phi_{P^-}^0$ and $\Delta\phi_{P^+}^0$ denote the standard potentials of formation of polarons. In eqs 2a and 2b, c_{P^+} and c_{P^-} denote the polaron concentrations close to the electrode, ϕ is the local electric potential, e is the fundamental charge, k is the Boltzmann constant, and T is the absolute temperature.

At zero bias, the polarons distribute homogeneously, and their concentrations are given by

$$c_{P^-} = c_{P^+} \approx c_m \exp(-eE_g/2kT) \equiv c_{Pi} \ll c_m \tag{3}$$

because $\Delta\phi_{P^-}^0 + \Delta\phi_{P^+}^0 = E_g/e \approx 2$ V. The interfacial potentials are then $\Delta_m^p\phi_i = (\Delta\phi_{P^-}^0 - \Delta\phi_{P^+}^0)/2$.

When a bias potential is applied, the equilibria 1a and 1b are displaced and $c_{P^-} \neq c_{P^+}$. At the cathode/polymer interface, $\Delta\phi_m^p$ is made more positive than $\Delta_m^p\phi_i$ so that c_{P^-}/c_{P^+} becomes greater than 1 according to the equilibrium equation

$$\Delta\phi_m^p = \Delta_m^p\phi_i + \frac{1}{2}\frac{kT}{e}\ln\frac{c_{P^-}}{c_{P^+}} \tag{4}$$

At the anode/polymer interface, opposite changes take place.

Without loss of generality, we take the electrode at $x = 0$ to be the cathode and write

$$c_{P^-}(0) \approx \frac{c_m}{1 + \exp[-e(\Delta_m^p\phi - \Delta\phi_{P^-}^0)/kT]} \tag{5a}$$

$$c_{P^+}(L) \approx \frac{c_m}{1 + \exp[-e(\Delta_p^{m'}\phi - \Delta\phi_{P^+}^0)/kT]} \tag{5b}$$

where the two metal electrodes have been identified as m and m′. The interfacial potentials are then $\Delta_m^p\phi \equiv \phi(0) - \phi^m$ and $\Delta_p^{m'}\phi \equiv \phi^{m'} - \phi(L)$. The concentrations $c_{P^+}(0)$ and $c_{P^-}(L)$ are given by eq 4.

(b) Polaron Transport and Recombination within the Active Layer. The electrode/polymer contacts are considered to be nonblocking; that is no charge-transfer resistance appears at these interfaces. The flow of the injected charges within the active layer is described by the drift−diffusion equations

$$J_{P^+} = -D_{P^+}\left(\frac{dc_{P^+}}{dx} + c_{P^+}\frac{e}{kT}\frac{d\phi}{dx}\right) \tag{6a}$$

$$J_{P^-} = -D_{P^-}\left(\frac{dc_{P^-}}{dx} - c_{P^-}\frac{e}{kT}\frac{d\phi}{dx}\right) \tag{6b}$$

and the steady-state continuity equations

$$\frac{dJ_{P^+}}{dx} = \frac{dJ_{P^-}}{dx} = -k_r c_{P^+} c_{P^-} \tag{6c}$$

where J_{P^+} and J_{P^-} denote the polaron flux densities (in cm^{-2} s^{-1}), D_{P^+} and D_{P^-} stand for the diffusion coefficients (in cm^2/s), which are assumed to be independent of the doping level, and k_r is the recombination rate constant (in cm^3 s^{-1}).

The processes of electron−hole recombination and singlet exciton formation, as well as the dynamics of excitons (decay, trapping, etc.), play a decisive role in determining the electroluminescence efficiency of LECs. Although significant advances have been recently achieved,[2,3,16] no conclusive theory is yet available. Therefore, eq 6c must be considered as a reasonable simplification that at least represents the trends in the real recombination process.

The electric field in eqs 6a and 6b is primarily determined by the local conductivity. The ion concentrations in the polymer electrolyte therefore become important here. To evaluate the electric field, the local electroneutrality assumption (see Appendix for a discussion of the validity of this assumption)

$$c_{P^+} + c_{C^+} = c_{P^-} + c_{A^-} \tag{7}$$

is used. Since the ion species cannot react at the electrodes, their concentrations are given by equilibrium Boltzmann distributions so that

$$\frac{e}{kT}\frac{d\phi}{dx} = -\frac{1}{c_{C^+}}\frac{dc_{C^+}}{dx} = \frac{1}{c_{A^-}}\frac{dc_{A^-}}{dx} \tag{8}$$

The integration of the second equality in eq 8 yields

$$c_{C^+}(x)\, c_{A^-}(x) = {c_{se}}^2 \tag{9}$$

where c_{se} is a constant that plays the role of an effective salt concentration. The redox processes at the electrodes imply a redistribution of the initially homogeneous ion concentrations. After this redistribution, there is a point inside the film where the two ion concentrations are still equal to each other, though smaller than the initial value c_s. Equation 9 requires the ion concentrations at this point to be c_{se}, and the difference between c_{se} and c_s increases with the doping level. Effective salt concentrations are also defined in the description of conducting polymer films immersed in electrolyte solutions,[14a,b] though they are related then to resolvation energies of ion components in their transfer from the solution to the film. Note, finally, that the ionic diffusion coefficients do not appear in the present steady-state formulation of the problem because of the zero ion flux condition.

From eqs 7 and 9, the anion concentration is

$$c_{A^-}(x) = c_{Pd}(x) + [{c_{Pd}(x)}^2 + {c_{se}}^2]^{1/2} \tag{10}$$

where $c_{Pd} \equiv (c_{P^+} - c_{P^-})/2$, while eq 8 can be written as

$$\frac{e}{kT}\frac{d\phi}{dx} = \frac{1}{({c_{Pd}}^2 + {c_{se}}^2)^{1/2}}\frac{dc_{Pd}}{dx} \tag{11}$$

Equation 11 implies that the electric potential drop inside the polymer film is negligible when the salt concentration is large (i.e., when the ion concentrations are larger than the polaron concentrations). In this case the applied potential difference is localized at the two electrode/polymer interfaces and polaron transport takes place mostly by diffusion. (This is the supporting electrolyte effect widely used in electrochemistry.)

The substitution of eq 11 into eqs 6a−6c leads to a system of two second-order ordinary differential equations, which require the specification of four boundary conditions for their solution. Two of them result from applying eq 4 to the interfaces at $x = 0$ and $x = L$. In practice, due to the large values of $\Delta\phi^0_{P^-}$ and $\Delta\phi^0_{P^+}$ (which can be estimated as $E_g/2e \approx$ 1 V), this is equivalent to setting $c_{P^+}(0) = c_{P^-}(L) = 0$ as boundary conditions.

A third boundary condition comes from the fact that the applied potential difference V is also known. This can be expressed as

$$V = \Delta^{m'}_{p}\phi + \phi(L) - \phi(0) + \Delta^{p}_{m}\phi \tag{12}$$

where the potential drop in the active layer

$$\phi(L) - \phi(0) = \frac{kT}{e}\ln\frac{c_{Pd}(L) + [{c_{Pd}(L)}^2 + {c_{se}}^2]^{1/2}}{c_{Pd}(0) + [{c_{Pd}(0)}^2 + {c_{se}}^2]^{1/2}} \tag{13}$$

is obtained from eqs 8 and 10.

The fourth boundary condition originates from the fact that the film is electrically neutral, so that the positive charge injected at the anode must equal the negative charge injected at the cathode. This is expressed as

$$\int_0^L c_{P^+}\, dx = \int_0^L c_{P^-}\, dx \tag{14}$$

This ends the mathematical formulation.

The solution of the boundary value problem must be obtained numerically. We make use of an iterative procedure starting with an initial guess for c_{se}, the system of differential equations is solved, and a better approximation to the exact value of c_{se} is obtained by requiring the total anion concentration to remain constant, i.e.,

$$\frac{1}{L}\int_0^L c_{A^-}\, dx = c_s \tag{15}$$

The procedure converges and the final solution are used to evaluate the electric current density

$$I = -e(J_{P^+} - J_{P^-}) \tag{16}$$

the peak recombination rate

$$r_{max} = (k_r c_{P^+} c_{P^-})_{max} \tag{17a}$$

the average recombination rate

$$r_{av} = \frac{1}{L}\int_0^L (k_r c_{P^+} c_{P^-})\, dx \tag{17b}$$

and the average level of doping

$$c_{P,av} \equiv \frac{1}{L}\int_0^L c_{P^-}\, dx \tag{18}$$

Note that the minus sign in eq 16 has been introduced so that $I > 0$ when $V > 0$ (i.e., here $I > 0$ denotes current flowing from electrode m′ to electrode m, and $V > 0$ indicates that the potential of electrode m′ is positive with respect to electrode m).

Also, a junction width Δx (i.e., the thickness of the region where most of the polaron recombination takes place) can be *defined* as the distance between the two outer positions where the local recombination rate equals the average value.

(c) Energy Diagrams. In the above sections we have followed the classical metal electrochemistry approach. In particular, eqs 1a and 1b have envisaged the conjugated chain segments as redox species that may undergo electrochemical reactions at the electrodes. However, the behavior of conjugated polymers is often described in terms of the energy level model of semiconductor physics. The connection between these two approaches is clear in a qualitative level. The standard potentials $\Delta\phi^0_{P^-}$ and $\Delta\phi^0_{P^+}$ reflect the tendency of the redox species to give up or accept an electron when they approach the electrode and therefore represent a measurement of the electronic energy levels on any of these species. The definition of Fermi levels, however, is not so straightforward.

Equations 2a and 2b result from the equality of electrochemical potentials of both sides of eqs 1a and 1b, respectively. The Fermi energy of the electrons in the metal is the same as their electrochemical potential,[17] so that we can calculate the Fermi energy of the electrode as determined by the interfacial potential and by the potential in solution. In fact, this equilibrium between the electrodes and the conjugated polymer allows for the introduction of an effective Fermi energy in the polymer as given by[18]

$$E_F(x) = -e[\phi(x) - \phi(0)] + \frac{1}{2}kT\ln\frac{c_{P^-}(x)}{c_{P^+}(x)} + \text{constant} \quad (19)$$

At $x = 0$ and $x = L$, the Fermi energy in the polymer equals the Fermi energy of the electrode, and eqs 4 and 12 then imply $E_F(L) - E_F(0) = -eV$, as should be expected.

The definition of effective Fermi energy shown in eq 19 is commonly used in electrochemical studies at semiconductor electrodes.[18] Alternatively, the nonequilibrium semiconductor physics approach can also be followed. In doing so, the cases of low and high level of doping will be analyzed separately, and we will concentrate on the interface at $x = 0$. Equation 5a closely resembles the Fermi−Dirac probability function

$$f(E) = \left(\frac{c_{P^-}(0)}{c_m}\right) = \frac{1}{1 + \exp[(E - E_F)/kT]} \quad (20)$$

The case of nondegenerate semiconductors, where $E - E_F >> kT$ and Maxwell−Boltzmann statistics can be used, is equivalent to that of low level of doping ($\Delta\phi^0_{P^-} - \Delta^p_m\phi >> kT$) where (see eq 3)

$$c_{P^-}(0) \approx c_{Pi}\exp[e(\Delta\phi^p_m - \Delta^p_m\phi_i)/kT] \quad (21a)$$

$$c_{P^+}(0) \approx c_{Pi}\exp[e(\Delta^p_m\phi_i - \Delta^p_m\phi)/kT] \quad (21b)$$

Within the conjugated polymer, a state of nonequilibrium exists for polarons of different charge, and this requires the use of different quasi-Fermi levels for differently charged species. The local polaron concentrations are then written as[19]

$$c_{P^-}(x) \equiv c_{Pi}\exp\{[E_{Fn}(x) - E_{Fi}(x)]/kT\} \quad (22a)$$

$$c_{P^+}(x) \equiv c_{Pi}\exp\{[E_{Fi}(x) - E_{Fp}(x)]/kT\} \quad (22b)$$

where E_{Fi} is the intrinsic Fermi level (i.e., that at zero bias), and E_{Fn} and E_{Fp} denote the quasi-Fermi levels for negative and positive polarons, respectively. At the metal/polymer interfaces, $E_{Fn} = E_{Fp}$. Within the polymer, however, $c_{P^-}c_{P^+} > c_{Pi}^2$ because of the electron and holes injected at the electrode/polymer interfaces, and therefore $E_{Fn} > E_{Fp}$.[19] The variation of the intrinsic Fermi level with position inside the polymer is taken as

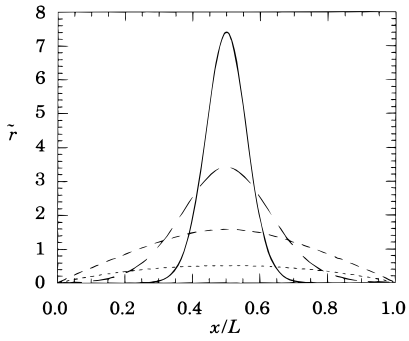

Figure 1. Recombination rate profile for $\tilde{c}_s = 1$, $D_{P^+} = D_{P^-}$, $\Delta^p_m\tilde{\phi} = 40$, and $\tilde{k}_r = 10$ (···), 10^2 (- --), 10^3 (— —), and 10^4 (—).

$$E_{Fi}(x) - E_{HOMO} = E_g/2 - e[\phi(x) - \phi(0)] \quad (23)$$

so that $E_{Fn}(L) - E_{Fn}(0) = -eV$ is again satisfied.

The case of high level of doping is equivalent to that of a degenerate semiconductor, where $E_F - E_{HOMO} > E_g$ and Fermi−Dirac statistics (eq 20) must be used.[19] It is then satisfied (see eqs 2a−5a) that

$$c_{P^-}(0)\,c_{P^+}(0) \approx \left(\frac{c_{Pi}}{1 + \exp[e(\Delta^p_m\phi - \Delta\phi^0_{P^-}]/kT)}\right)^2 \quad (24)$$

and eqs 22a and 22b must be replaced by

$$c_{P^-}(x) \equiv c_{Pi}\frac{\exp\{[E_{Fn}(x) - E_{Fi}(x)]/kT\}}{1 + \exp\{[E_{Fn}(0) - E_{Fi}(0) - E_g/2]/kT\}} \quad (25a)$$

$$c_{P^+}(x) \equiv c_{Pi}\frac{\exp\{[E_{Fi}(x) - E_{Fp}(x)]/kT\}}{1 + \exp\{[E_{Fn}(0) - E_{Fi}(0) - E_g/2]/kT\}} \quad (25b)$$

where $E_{Fn}(0) - E_{Fi}(0) = E_{Fi}(L) - E_{Fn}(L)$, and $E_{Fn} = E_{Fp}$ at the metal/polymer interfaces. Equation 4 now yields

$$E_{Fn}(0) = E_{Fi}(0) + e(\Delta^p_m\phi - \Delta^p_m\phi_i) \quad (26a)$$

$$E_{Fn}(L) = E_{Fi}(L) - e(\Delta^{m'}_p\phi - \Delta^{m'}_p\phi_i) \quad (26b)$$

where $\Delta^{m'}_p\phi_i \equiv -\Delta^p_m\phi_i$. It is now observed that when $\Delta^p_m\phi_i - \Delta\phi^0_{P^-} > 0$, then $\Delta^p_m\phi - \Delta^p_m\phi_i > E_g/2$ and $E_{Fn}(0) - E_{HOMO} > E_g$; that is, the Fermi level gets into the "conduction band" (as in the case of degenerate semiconductors). Evidently, the relation $E_{Fn}(L) - E_{Fn}(0) = -eV$ is still satisfied.

Finally, substituting eqs 25a and 25b into eq 19, the effective Fermi level is identified as the average of the quasi-Fermi levels

$$E_F(x) = \frac{E_{Fn}(x) + E_{Fp}(x)}{2} \quad (27)$$

and the constant in eq 19 becomes $E_{HOMO} + E_g/2$.

3. Results

We present several series of results in order to understand the influence of the different system parameters, namely, the ratio of polaron diffusion coefficients D_{P^+}/D_{P^-}, the recombination rate constant k_r, the salt concentration c_s, and the applied potential difference V. The standard potentials for the formation of polarons $\Delta\phi^0_{P^-}$ and $\Delta\phi^0_{P^+}$ are kept fixed at 40 kT/e and denoted simply by $\Delta\phi^0_P$. The value of kT/e at room temperature is approximately 0.025 V, which makes this value of

TABLE 1: Effect of the Recombination Rate Constant for $\tilde{c}_s = 1$, $D_{P^+} = D_{P^-}$, and $\Delta_m^p\tilde{\phi} = 40$

$\tilde{k}_r$	$\tilde{c}_{se}$	$\tilde{V}$	$\tilde{I}$	$\tilde{r}_{av}$	$\tilde{r}_{max}$	$\Delta x/L$	$\tilde{c}_{P,av}$
10	0.989 53	80.500	1.236	0.348	0.515	0.582	0.236
10^2	0.989 28	80.500	1.171	0.965	1.583	0.538	0.172
10^3	0.989 09	80.500	1.135	1.134	3.421	0.391	0.139
10^4	0.989 02	80.500	1.127	1.127	7.410	0.238	0.131

$\Delta\phi_P^0$ correspond to an onset voltage of ca. 2 V (in agreement with experimental observations).[4]

The results are presented in terms of the following dimensionless variables:

$$\tilde{c}_i \equiv c_i/c_m \ (i = P^+, P^-, P^0, C^+, A^-, s, se, ...) \quad (28a)$$

$$\tilde{k}_r \equiv k_r c_m L^2/D_{Ps} \quad (28b)$$

$$\tilde{r} \equiv rL^2/D_{Ps}c_m \quad (28c)$$

$$\tilde{I} \equiv IL/eD_{Ps}c_m \quad (28d)$$

$$\tilde{V} \equiv eV/kT, \quad \tilde{\phi} \equiv e\phi/kT \quad (28e)$$

$$\tilde{E}_i \equiv E_i/kT \ (i = F, Fn, Fp, ...) \quad (28f)$$

where

$$D_{Ps} \equiv 2D_{P+}D_{P-}/(D_{P+} + D_{P-}) \quad (28g)$$

is an appropriate average polaron diffusion coefficient.

(a) Effect of the Recombination Constant. Figure 1 shows the effect of $\tilde{k}_r$ on the recombination rate profile. Table 1 gives the values of the effective salt concentration, the bias potential, the electric current density, the average recombination rate, the peak recombination rate, the junction width, and the average level of doping.

It can be seen here that the recombination rate constant greatly influences both the junction width and the peak value of the recombination rate, while the other parameters shown in Table 1 are practically independent of it. For instance, the dimensionless bias potential remains constant at 80.500 (slight changes in the sixth significant figure exist), and this is distributed as 40.000, 0.500, 40.000 (interfacial potential drop, film potential drop, interfacial potential drop). The average recombination rate is only slightly affected by $\tilde{k}_r$, since the recombination rate profile becomes thinner and higher at the same time.

(b) Junction Position. Carrier mobilities in π-conjugated polymers are not well-known, but there is good evidence that holes are more mobile than electrons in PPV.[2] The junction position is then expected to be off-center and closer to the cathode. Thus, a reversal of polarity should lead to the change of position of this junction in order to keep it closer to the cathode. These observations have been reported in refs 4, 6, 7, and 9. (In ref 4, the junction position was observed closer to the anode, although it moved toward the cathode during continuous operation.)

Previous studies of the position of the recombination zone have dealt with the case of negligible migrational contribution to electron transport, where simple analytical expressions can be obtained.[20] In the present study, however, the junction position must be studied by numerical solution of the transport equations. To show the effect of D_{P^+}/D_{P^-} on the recombination rate profile, some calculations were made for $\tilde{c}_s = 1$, $\tilde{k}_r = 10^3$, and $\tilde{V} = 83.000$. When $D_{P^+} = D_{P^-}$, the recombination peak appeared centered ($x = 0.5L$) as shown in Figure 1. On the contrary, when $D_{P^+}/D_{P^-} = 4$ (which is close to the ratio estimated for polarons in polyacetylene[21] at room temperature), the peak appeared closer to the cathode at $x = 0.32L$. The less realistic value $D_{P^+}/D_{P^-} = 1/4$ shifted the recombination peak toward the anode by the same amount, i.e., to $x = 0.68L$.

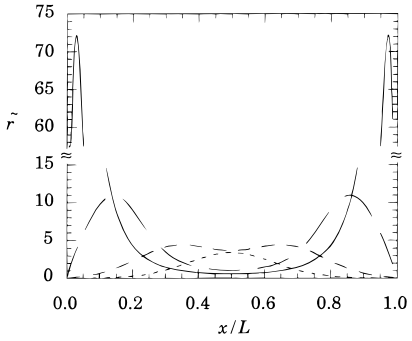

Figure 2. Recombination rate profile for $\tilde{k}_r = 10^3$, $D_{P^+} = D_{P^-}$, $\Delta_m^p\tilde{\phi} = 40$, and $\tilde{c}_s = 1$ (···), 0.1 (---), 0.05 (− −), and 0.01 (—).

To facilitate the interpretation of the results, we will restrict consideration to the case $D_{P^+} = D_{P^-}$.

(c) Effect of the Salt Concentration. Figure 2 shows the effect of $\tilde{c}_s$ on the recombination rate profile. Since the molar ratio of lithium salt to ethylene oxide units in PEO was 0.05:1 in refs 4−9, the value of $\tilde{c}_s$ in these LECs is expected to be somewhat less than 0.05 (ion−polaron association effects, which have been neglected here, could contribute to lower the effective salt concentration). Table 2 shows the values of the relevant variables, while the corresponding ion concentration profiles, polaron concentration profiles, and electric potential profiles are shown in Figures 3a−d and 4. Note that the electric potential profiles have been scaled by a factor $\tilde{c}_s$.

It is observed here that the salt content is a very important parameter, influencing all the variables considered in Table 2. In particular, the salt content determines the (dimensionless) potential drop inside the film (which can be estimated from Table 2 as 0.500, 9.080, 40.908, and 416.49 when $\tilde{c}_s$ changes from 1 to 0.01, respectively, since the sum of the two interfacial drops is kept constant at 80.000). This, in turn, affects the drift of polarons inside the film and the electric current density. Notice that the potential drop inside the film is only significant when $c_s < c_m$.

The shape of the recombination rate profiles in the case of low salt content shown in Figure 2 deserves some comments. Figures 3c and 3d show that the ions accumulate close to the electrodes when the doping level increases. The larger values of the product of polaron concentrations are then present close to the electrodes and hence the resulting recombination profile. The physical reason for this fact can be found in eqs 8 and 11, which require the gradients of c_{Pd} and c_{C^+} to be similar, except for the sign, in the case of low salt content. If no P^+ polarons were present close to the cathode, $c_{Pd} \approx -c_{P^-}/2$, and local electroneutrality would require the concentrations of C^+ and P^- to be similar and, hence, their gradients also. Since these two relations between the concentration gradients of C^+ and P^- cannot be fulfilled simultaneously, some P^+ polarons have to be present close to the cathode.

(d) The Current−Voltage Characteristics. Figure 5 shows the current−voltage characteristics for different values of $\tilde{c}_s$ and $\tilde{k}_r$. The bias potential range here considered has been chosen in order to facilitate the comparison with the experimental results presented in refs 5, 7, and 8, since 160 kT/e units is ca. 4 V at room temperature.

The current−voltage characteristics for $\tilde{c}_s = 0.1$, $\tilde{k}_r = 10^2$ and $\tilde{c}_s = 0.1$, $\tilde{k}_r = 10^3$ show well-defined limiting current

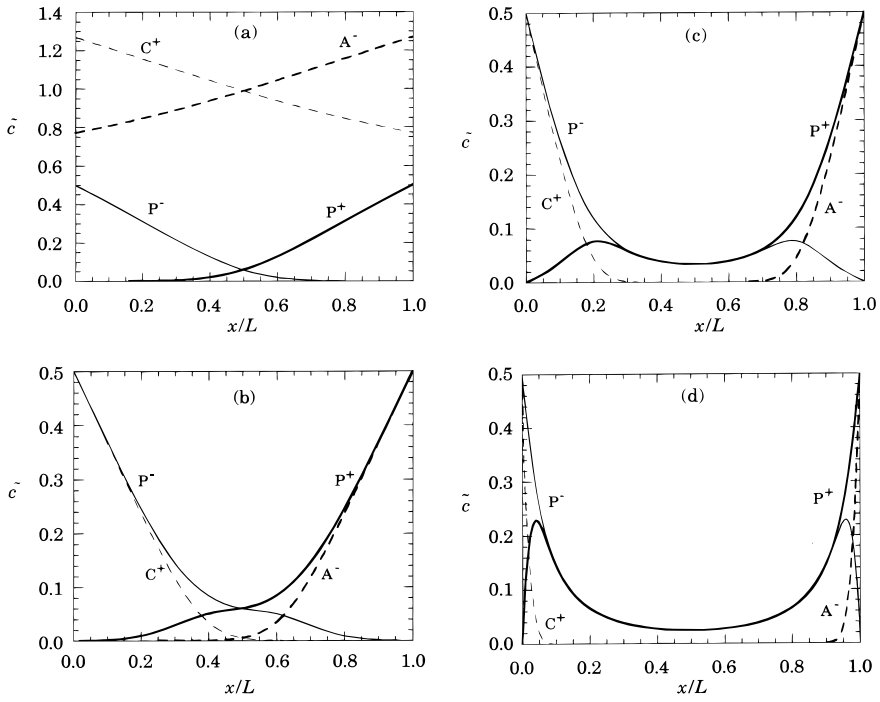

Figure 3. Ion and polaron concentration profiles for $\tilde{k}_r = 10^3$, $D_{P^+} = D_{P^-}$, $\Delta_m^p\tilde{\phi} = 40$, and $\tilde{c}_s = 1$ (a), 0.1 (b), 0.05 (c), and 0.01 (d).

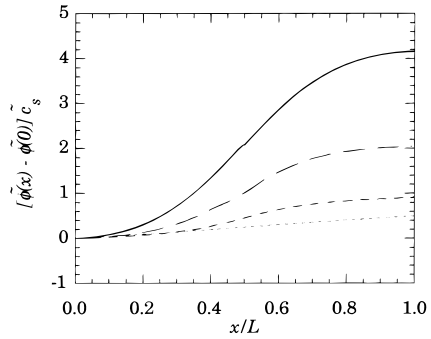

Figure 4. Electric potential profile for $\tilde{k}_r = 10^3$, $D_{P^+} = D_{P^-}$, $\Delta_m^p\tilde{\phi} = 40$, and $\tilde{c}_s = 1$ (···), 0.1 (---), 0.05 (− −), and 0.01 (—).

TABLE 2: Effect of the Salt Concentration for $\tilde{k}_r = 10^3$, $D_{P^+} = D_{P^-}$, and $\Delta_m^p\tilde{\phi} = 40$

$\tilde{c}_s$	$\tilde{c}_{se}$	$\tilde{V}$	$\tilde{I}$	$\tilde{r}_{av}$	$\tilde{r}_{max}$	$\Delta x/L$	$\tilde{c}_{P,av}$
1	0.9891	80.500	1.135	1.134	3.421	0.391	0.1389
0.1	5.337×10^{-3}	89.080	2.661	2.639	4.448	0.565	0.1233
0.05	6.546×10^{-10}	120.91	5.724	5.096	10.951	0.916	0.0955
0.01	1.815×10^{-91}	496.49	39.184	12.344	72.186	0.992	0.0868

densities. The same behavior is expected in the case $\tilde{c}_s = 0.05$ and $\tilde{k}_r = 10^3$, though the limiting current density will be reached at a bias potential much higher than those shown in Figure 5. Later we show how to estimate this bias potential. The reason for the existence of a limiting current can be found in eqs 2, 12, and 13. Since the polaron concentrations must be smaller than c_m, the Nernst equations (eqs 2a and 2b) cause the dependence of the interfacial doping level on the interfacial potential to exhibit a saturation behavior.[14]

To show how the applied potential is distributed in the system, Figure 6 plots the variation of the potential drop inside the film, as well as the effective salt concentration with the applied voltage. The interfacial potential drops (both of equal magnitude) can then be estimated as $[\tilde{V} - \tilde{\phi})(L) + \tilde{\phi})(0)]/2$. Figure 6 shows a striking coincidence between the variation with the applied voltage of the effective salt concentration and the potential drop inside the film. In the case of low salt content

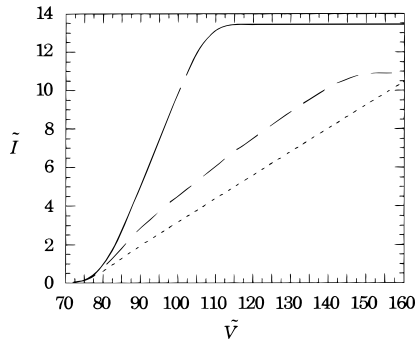

Figure 5. Current−voltage curves for $\tilde{c}_s = 0.05$, $\tilde{k}_r = 10^3$ (···), $\tilde{c}_s = 0.1$, $\tilde{k}_r = 10^3$ (---), and $\tilde{c}_s = 0.1$, $\tilde{k}_r = 10^2$ (—).

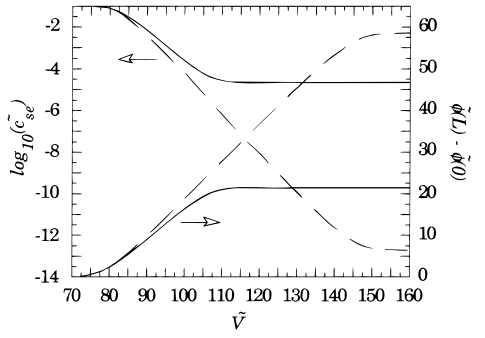

Figure 6. Effective salt concentration and potential drop inside the active layer for $\tilde{c}_s = 0.1$, $\tilde{k}_r = 10^3$ (---) and $\tilde{c}_s = 0.1$, $\tilde{k}_r = 10^2$ (—).

($c_{se} << c_{Pd}(0)$, $c_{Pd}(L)$), eq 13 reduces to

$$\tilde{\phi}(L) - \tilde{\phi}(0) \approx \ln \frac{2c_{Pd}(L)}{c_{se}^2/2|c_{Pd}(0)|} \approx 2 \ln \frac{2c_{Pd}(L)}{c_{se}} \quad (29)$$

which shows the proportionality between $\tilde{\phi}(L) - \tilde{\phi}(0)$ and ln c_{se} observed in Figure 6; note that $c_{Pd}(0) \approx -c_{Pd}(L)$. It is still necessary to provide a physical explanation of the dependence of c_{se} on the applied voltage. The constant electric field

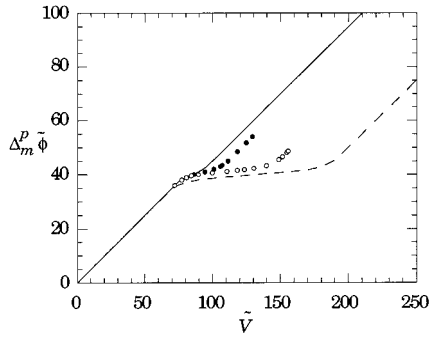

Figure 7. Interfacial potential drop determined from the constant electric field approximation for $\tilde{c}_s = 0.01$ (•••), $\tilde{c}_s = 0.1$ (—), and from the numerical solutions in Figure 5 for $\tilde{c}_s = 0.1$, $\tilde{k}_r = 10^2$ (○) and $\tilde{c}_s = 0.1$, $\tilde{k}_r = 10^3$ (●).

approximation (i.e., the approximation that the field is constant within the polymer layer) is helpful in this respect. Using this approximation, the boundary value problem can be solved analytically, and it can be shown that

$$c_{se} \equiv c_s \frac{\tilde{\phi}(L) - \tilde{\phi}(0)}{2 \sinh[(\tilde{\phi}(L) - \tilde{\phi}(0))/2]} \tag{30}$$

The solution to eqs 2, 29, and 30 shows that when the salt content is high, saturation is reached at low applied voltages, and the maximum potential drop inside the active layer is small. In fact, the limit of eqs 29 and 30 when $\tilde{\phi}(L) - \tilde{\phi}(0) >> 1$ (which also implies $2c_{Pd}(L) \approx c_m$) yields the result

$$[\tilde{\phi}(L) - \tilde{\phi}(0)]_{max} = 1/\tilde{c}_s \tag{31}$$

The value of the applied voltage at which saturation is reached can also be estimated from the series expansion of eqs 29 and 30 around $\Delta_m^p\tilde{\phi} = \Delta\tilde{\phi}_P^0$ as

$$\tilde{V}_{saturation} \approx 2\Delta\tilde{\phi}_P^0 + 4 + 1/\tilde{c}_s = 84 + 1/\tilde{c}_s \tag{32}$$

The physical reason for this early saturation, at high $\tilde{c}_s$, lies in the fact that a large electric field cannot be sustained within a highly conducting medium, i.e., the "supporting electrolyte" principle. Note that the saturation mentioned here refers to the potential drop inside the film and should not be confused with the attainment of the limiting current density.

The dependence of the interfacial potential drop, $[\tilde{V} - \tilde{\phi}(L) + \tilde{\phi})(0)]/2$, on the applied voltage is also very interesting. When the applied voltage is so low that no doping takes place, the applied voltage fractionates into two equal parts at the two electrode/polymer interfaces. Doping is initiated when the applied potential is about 10 kT/e units below $2\Delta\phi_P^0$. The interfacial doping level then increases gradually while most of the increase in the applied voltage concentrates inside the active layer. After saturation of the potential drop within this layer, the interfacial potential drops begin to increase again and finally reach interfacial doping levels close to 100%. Figure 7 depicts this situation for two values of $\tilde{c}_s$. Some values of the interfacial potential drop corresponding to the numerical solutions presented in Figure 5 are also shown for comparison.

Thus far we have described in some detail the origin of the limiting current in terms of the applied voltage. It is now worthwhile to return to Figure 5 and attempt to estimate the limiting current density. We see in Figure 5 that the limiting current increases with decreasing $\tilde{c}_s$. A similar trend is observed in Table 2, where the current density for a fixed interfacial doping level of 50% (or fixed interfacial potential drop $\Delta_m^p\tilde{\phi} = \Delta\tilde{\phi}_P^0 = 40$) assumed a value close to 1 when the salt content was high and increased with decreasing $\tilde{c}_s$ for low salt content. These observations can be rationalized in terms of eqs 6, 11, and 16. In the case of high salt content, polaron transport takes place primarily by diffusion so that

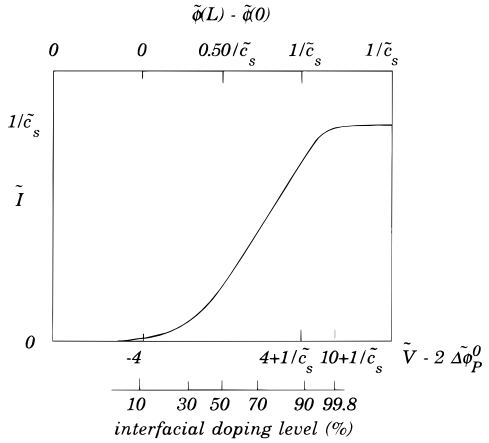

Figure 8. Schematic current−voltage curve of a low salt content LEC.

$$\tilde{I} \approx \tilde{c}_{P+}(L) - \tilde{c}_{P-}(L) - \tilde{c}_{P+}(0) + \tilde{c}_{P-}(0) \approx 2\tilde{c}_{P-}(0) \tag{33}$$

where the fact $\tilde{c}_{P^+}(L) \approx \tilde{c}_{P^-}(0) >> \tilde{c}_{P^+}(0) \approx \tilde{c}_{P^-}(L)$ has been used. Table 2 shows that eq 33 is satisfied in the high salt content limit, since the interfacial potential drop $\Delta_m^p\tilde{\phi}$ has been set equal to $\Delta\tilde{\phi}_P^0$ in Table 2, and $2\tilde{c}_{P^-}(0)$ equals 1 in this case.

In the case of low salt content, it can be easily proved from eqs 6, 11, and 16 that

$$I = 2eD_P\left[1 + \frac{c_{P+} + c_{P-}}{2(c_{Pd}^2 + c_{se}^2)^{1/2}}\right]\frac{dc_{Pd}}{dx} \approx 2eD_P\left(1 + \frac{c_{P+} + c_{P-}}{|c_{P+} - c_{P-}|}\right)\frac{dc_{Pd}}{dx} \tag{34}$$

At $x = 0$, eq 34 reduces to

$$I \approx 4eD_P\left(\frac{dc_{Pd}}{dx}\right)_{x=0} \approx -2eD_P\left(\frac{dc_{C^+}}{dx}\right)_{x=0} \tag{35}$$

where the local electroneutrality condition has been used. Since the cation concentration distribution can be described in this case as approximately linear (see, for example Figure 3d), and varying from $c_{P^-}(0)$ at $x = 0$ to approximately zero at a position x_0, so that eq 15 (for cations) fixes the value of x_0 as $2c_sL/c_{P^-}(0)$, the dimensionless electric current density can be estimated as

$$\tilde{I} \approx \tilde{c}_{P-}(0)^2/\tilde{c}_s \tag{36}$$

The limiting current density would correspond to maximum doping ($c_{P^-}(0) = 1$) and could then be estimated as $1/\tilde{c}_s$, which in the case of Figure 5 would amount to 10 for the case $\tilde{c}_s = 0.1$ and $\tilde{k}_r = 10^2$. The small difference between the limiting current density observed in Figure 5 and these values is due to the assumption of a linear cation concentration profile; the actual profile is steeper at $x = 0$.

As a summary of this section, Figure 8 reproduces the general trends of a current−voltage curve in the low salt concentration regime. Even though this figure offers a good description of the qualitative behavior, it should not be used for quantitative purposes since it underestimates both the current density and

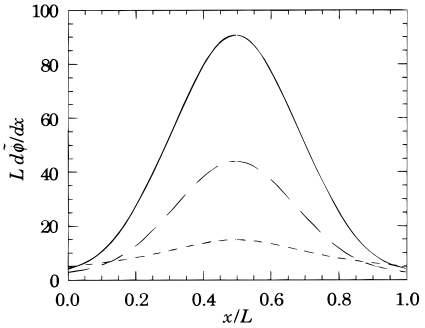

Figure 9. Electric field profile corresponding to $\tilde{c}_s = 0.05$, $\tilde{k}_r = 10^3$, and $\tilde{V} = 80.73$ (---), 120.91 (− −), and 166.39 (—).

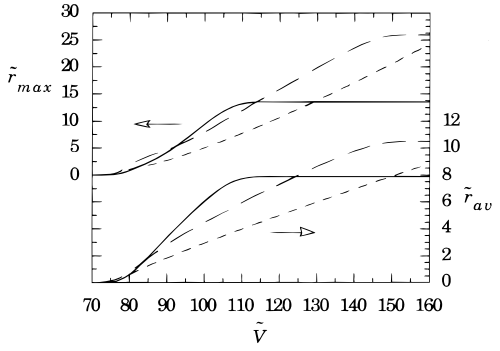

Figure 10. Photoemission−voltage curves for $\tilde{c}_s = 0.05$, $\tilde{k}_r = 10^3$ (---), $\tilde{c}_s = 0.1$, $\tilde{k}_r = 10^3$ (− −), and $\tilde{c}_s = 0.1$, $\tilde{k}_r = 10^2$ (—).

the potential differences. It is worth noting that Figures 7 and 8 have been obtained with the use of the constant electric field approximation, which is only valid when the recombination rate constants are small, and not for the constants used in the computations presented in Figures 5 and 6 (see also Figure 4 and Figure 9).

It is also interesting to note that Figure 8 suggests that threshold voltages should be determined from current−voltage curves in dimensionless form or, at least, by plotting the product *IL* against *V*. The slight increase in the threshold voltage with polymer film thickness reported in ref 4 would have been very likely avoided by this procedure.

(e) The Electric Field Profile. In an attempt to learn more about the nature of the junction in biased LECs, the electric field profile within the junction was recently measured by the OBIC method.[9] Figure 9 shows the electric field profile corresponding to some of the numerical solutions included in Figure 5, in particular, to those corresponding to $\tilde{c}_s = 0.05$, $\tilde{k}_r = 10^3$, and $\tilde{V} = 80.73$, 120.91, and 166.39, or, equivalently, 1.74 V, 2.61 V, and 3.59 V at 250 K. These plots are in qualitative agreement with Figure 2 of ref 9.

Note that the electric field is rather inhomogeneous for the larger applied potentials. This implies that the constant field assumption is expected to fail under these conditions. It can also be observed from Figures 4 and 7 that the constant field assumption fails in the cases of low salt content and large recombination rate constant. In spite of its restricted validity, this assumption is a useful tool to understand the basic trends of the system.

(f) Photoemission−Voltage Characteristics. Figure 10 exhibits the computed peak and average recombination rate curves corresponding to Figure 5. Since a fraction of the polaron recombination is considered radiative, the average recombination rate curves should be representative of the photoemission−voltage characteristics of the LEC.

It can be seen from Figures 5 and 10 that $\tilde{I}$ is approximately equal to $\tilde{r}_{av}$ for a given choice of parameters $\tilde{c}_s$, $\tilde{k}_r$, and $\tilde{V}$. This approximation is very good in the cases $\tilde{c}_s = 0.05$, $\tilde{k}_r = 10^3$ and $\tilde{c}_s = 0.1$, $\tilde{k}_r = 10^3$, while it becomes poorer in the case $\tilde{c}_s = 0.1$ and $\tilde{k}_r = 10^2$. Indeed, Table 1 shows that $\tilde{I} \approx \tilde{r}_{av}$ when $\tilde{k}_r$ is large, while a significant departure from this result appears for $\tilde{k}_r \leq 10^2$. Similarly, Table 2 shows that $\tilde{I} \approx \tilde{r}_{av}$ in the case of high salt content. The behavior appearing in Figures 5 and 10 is thus confirmed by the earlier calculations.

The integration of eq 6c together with the consideration of symmetry leads to the result

$$r_{av} = L[J_{p+}(L) - J_{p+}(0)] \approx L\,[J_{p+}(L) + J_{p-}(L)] \quad (37)$$

while for $x = L$ eq 16 reduces to

$$I = -e[J_{p+}(L) - J_{p-}(L)] \quad (38)$$

where $J_{P^+}(L) < 0$ and $J_{P^-}(L) > 0$. In the case of high salt content and large recombination rate constant, $|J_{P^+}(L)| >> J_{P^-}(L)$ (see the polaron concentration gradients at $x = L$ in Figures 3a−d), and the approximation $\tilde{I} \approx \tilde{r}_{av}$ becomes apparent.

(g) Junction Width. In the case of high salt content, where there is no splitting of the recombination rate profile, it is observed that the junction width narrows with increasing applied voltage, in agreement with the observations reported in ref 9. In the case of low salt content, the increase in applied voltage leads to a separation of the recombination rate profile into two zones, similar to what was previously observed in Figure 2. Nevertheless, in this case, the thickness of the zone in which recombination is important also narrows with increasing bias potential.

In the case of low salt content, a large recombination rate constant (larger than those considered here), and high applied voltage, a situation considered to be of practical interest, the junction width could amount to a few tenths of the polymer film thickness, in agreement with experimental observation.

(h) Energy Diagrams. Figure 11 shows the energy diagrams corresponding to the electric field profiles depicted in Figure 9, i.e., $\tilde{c}_s = 0.05$, $\tilde{k}_r = 10^3$, and $\tilde{V} = 80.73$, 120.91, and 166.39. Table 3 shows some additional information on these diagrams. The effective Fermi level and the quasi-Fermi levels have been calculated from eqs 19 and 25, respectively. It is observed that the difference between the quasi-Fermi levels is of the order of the semiconductor gap. Since this difference is related to the excess concentration of polarons (with respect to the zero bias case), it is observed that the difference increases with the applied potential (i.e., with the amount of charge injected). Also, since $\tilde{c}_{P^-}(L/2) = \tilde{c}_{P^-}(L/2) \approx \tilde{k}_r^{1/2}$, the difference $E_{Fn}(L/2) - E_{Fp}(L/2)$ decreases with increasing $\tilde{k}_r$.

Finally, it is interesting to observe that the effective Fermi level reaches the LUMO level at $x = 0$ when $\Delta_m^p\tilde{\phi} = \Delta\tilde{\phi}_p^0 = 40$, which corresponds to Figure 11b. Higher interfacial potential, as in Figure 11c, results in an effective Fermi level above the LUMO level in the cathodic region and below the HOMO level in the anodic region.

4. Conclusions

The model presented here provides a sound basis for the understanding of the performance of light-emitting electrochemical cells, which are now shown to behave like a forward biased p−i−n junction with inhomogeneously doped p- and n-type regions.

When a small potential difference is applied to the electrodes, it separates into parts, each localized at one of the polymer/electrode interfaces, so that the same level of doping (n-type at

TABLE 3: Additional Information on the Energy Diagrams Shown in Figure 11

$\tilde{V}$	$\tilde{c}_{se}$	$\tilde{\phi}(L) - \tilde{\phi}(0)$	$\tilde{c}_{P,av}$	$\tilde{E}_F(0) - \tilde{E}_{LUMO}(0)$	$\tilde{c}_{P^-}(0)$	$\tilde{E}_{Fn}(L/2) - \tilde{E}_{Fp}(L/2)$	$\tilde{c}_{P^-}(L/2)$
80.73	2.467×10^{-3}	3.901	0.0522	−1.586	0.170	73.67	0.0350
120.91	6.546×10^{-10}	40.908	0.0955	0.000	0.500	74.54	0.0326
166.39	2.698×10^{-16}	84.775	0.1118	0.806	0.691	75.40	0.0310

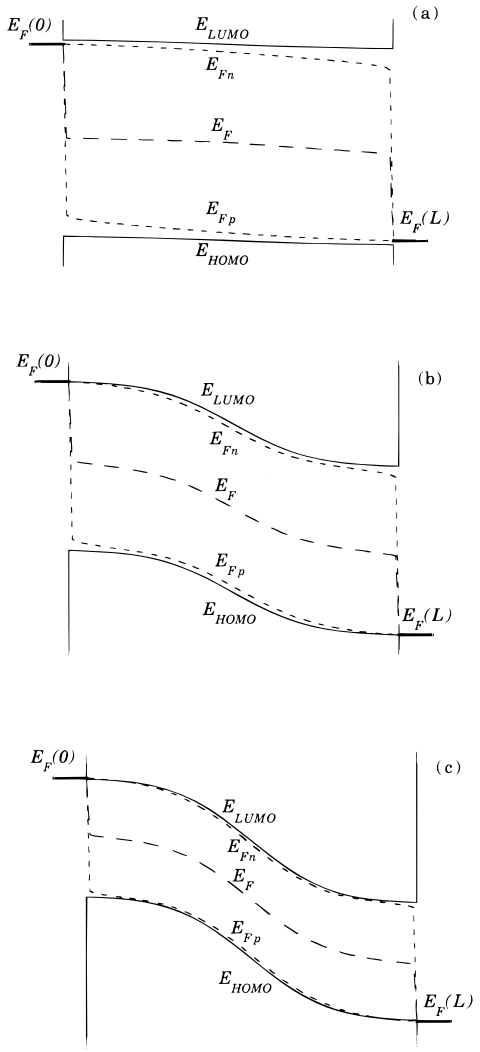

Figure 11. Energy diagrams for the cases considered in Figure 9, i.e., $\tilde{c}_s = 0.05$, $\tilde{k}_r = 10^3$ and $\tilde{V}) = 80.73$ (a), 120.91 (b), and 166.39 (c).

the cathode and p-type at the anode) is reached at both interfaces. The ion species then move within the polymer film so as to maintain local electroneutrality.

For larger applied potential, the doping level increases and the redistribution of ion species gives rise to a potential drop within the active layer, which also affects the transport of polarons. Large enough bias potentials lead to a depletion of ion species in the central region of the polymer film, which then resembles an intrinsic semiconductor. In this region, positively charge polarons moving toward the cathode, and negatively charged polarons moving toward the anode meet and recombine radiatively.

The model explains most of the experimental observations. In particular, it shows that junction formation is a *bulk* process related to electrodiffusion and recombination of polarons, and this explains its macroscopic nature. Calculated current−voltage and photoemission−voltage characteristics agree qualitatively with experiment. Observed changes with the applied voltage in junction width and the electric field profile are also accounted for. The average doping levels computed here are slightly greater than those calculated in ref 4, but since the experimental method employed there was expected to underestimate the doping level, the agreement is also considered satisfactory.

Even though the theory accurately predicts several observations that have been made with LECs, some of the assumptions should be critically considered. Thus, ion pairing has been neglected here. This phenomenon could probably occur in LECs and would affect the polaron standard potentials. Furthermore, the redox processes associated with forming an ion-paired polaron could be quite different from those presented here, and the current in such a device could be limited by the available counterions.[22]

Also, it is worthwhile to add some comments on the metal/polymer interface. It is well known that an interfacial layer is formed between the metallic electrodes and the conjugated polymer. The nature of this contact region is known to be of importance to the charge injection mechanism.[23] The results presented in Figures 5 and 7 can also throw some light on the details of this layer. It is concluded from these figures that, as long as the limiting current is not reached, the interfacial potential drop remains of the order of the standard potential for polaron formation. For the case considered here, this amounts to some 40 kT/e units. This large interfacial potential requires the presence of a space charge region where only ions are present (cations in the vicinity of the cathode and anions in the vicinity of the anode). The thickness of these regions can be estimated to be a few tens of angstroms and the ion concentrations there do not follow a Boltzmann distribution, except for a diffuse part in the outer end of the space charge region. Instead the ions accummulate there at the maximum possible concentration determined by packing considerations. This picture differs from the classical Stern picture in that the compact layer is wider than single molecule thickness. The presence of these space charge regions influences the charge injection mechanism; this is an open problem that needs further study. However, the space charge regions do not affect polaron transport and recombination within the active layer, and therefore the conclusions drawn in this work hold.

Future work on this subject should consider transient behavior, and numerical algorithms for the solutions of the partial differential equations that determine it should be developed. Also, experiments on the effect of the salt concentration on steady-state current−voltage and photoemission−voltage curves should be studied. Experimental work to check the inhomogeneity of the doping profile is currently in process.

Acknowledgment. J.A.M. thanks the Generalitat Valenciana for financial support. We are grateful to Darryl L. Smith and Mikhail A. Vorotyntsev for stimulating discussions.

Appendix

The local electroneutrality assumption is a widely used approximation to Poisson's equation in the solution of transport problems. It is expected to hold true in the bulk of any medium having a sufficiently high concentration of mobile charged species, and it is expected to fail in media where the electric field is rapidly varying and local concentrations may go to very low values.

M. Planck was the first to realize that the validity of the local electroneutrality assumption in transport problems could be tested by the calculation of the so-called residual charge.[24] If the electrostatic potential satisfies Poisson's equation, local electroneutrality would imply that the potential distribution would be linear. Yet the solutions for the potential obtained from the transport equations with the assumption of electroneutrality are not straight lines. This inconsistency can be explained by noting that the space charge required to generate the changes in the electric field within the polymer film,

$$\rho \equiv -\epsilon \frac{d^2\phi}{dx^2} \tag{39}$$

although not zero, is small compared to the balanced charge $e(c_{C^+} + c_{P^+}) = e(c_{A^-} + c_{P^-})$ at every point within the cell. This means that the solutions determined using the local electroneutrality assumption represent good self-consistent approximate solutions to the transport equations, and it provides a sort of a posteriori justification for setting the charge density equal to zero.[25] Although this consistency argument does not provide an analytical explanation for why the electroneutrality assumption should be made in the first place, it is widely accepted as a sound mathematical approximation.[26]

The validity of the local electroneutrality assumption has been checked for every calculation in this paper as described above. It emerges that the assumption becomes questionable in the case of low salt content, large recombination rate constant, and large bias potential. Numerical solutions under these conditions should employ Poisson's equation.

References and Notes

(1) (a) Berggren, M.; Inganäs, O.; Gustafsson, G.; Rasmusson, J.; Andersson, M. R.; Hjertberg, T.; Wennerström, O. *Nature* **1994**, *372*, 444. (b) Parker, I. D. *J. Appl. Phys.* **1994**, *75*, 1656. (c) Braun, D.; Heeger, A. J. *Appl. Phys. Lett.* **1991**, *58*, 1982. (d) Burroughes, J. H.; Bradley, D. D. C.; Brown, A. R.; Marks, R. N.; Mackay, K.; Friend, R. H.; Burns, P. L.; Holmes, A. B. *Nature* **1990**, *347*, 539.

(2) Halls, J. J. M.; Baigent, D. R.; Cacialli, F.; Greenham, N. C.; Friend, R. H.; Moratti, S. C.; Holmes, A. B. *Thin Solid Films* **1996**, *276*, 13.

(3) Vestweber, H.; Bässler, H.; Grüner, J.; Friend, R. H. *Chem Phys. Lett.* **1996**, *256*, 37.

(4) Pei, Q.; Yang, Y.; Yu, G.; Zhang, C.; Heeger, A. J. *J. Am. Chem. Soc.* **1996**, *118*, 3922.

(5) Cao, Y.; Yu, G.; Heeger, A. J.; Yang, C. Y. *Appl. Phys. Lett.* **1996**, *68*, 3218.

(6) Yang, Y.; Pei, Q. *Appl. Phys. Lett.* **1996**, *68*, 2708.

(7) (a) Pei, Q.; Yu, G.; Zhang, C.; Yang, Y.; Heeger, A. J. *Science* **1995**, *269*, 1086. (b) Bard, A. J. *Science* **1996**, *270*, 718. (c) Pei, Q.; Yu, G.; Zhang, C.; Yang, Y.; Heeger, A. J. *Science* **1996**, *270*, 719.

(8) Yu, G.; Yang, Y.; Cao, Y.; Pei, Q.; Zhang, C.; Heeger, A. J. *Chem. Phys. Lett.* **1996**, *259*, 465.

(9) Dick, D. J.; Heeger, A. J.; Yang, Y.; Pei, Q. *Adv. Mater.* **1996**, *8*, 985.

(10) (a) Bruce, P. G., Ed. *Solid State Electrochemistry*; Cambridge University Press: New York, 1995. (b) Lindford, R. G., Ed. *Electrochemical Science and Technology of Polymers, vol. 1*; Elsevier: New York, 1987.

(11) (a) Watanabe, M.; Wooster, T. T.; Murray, R.W. *J. Phys. Chem.* **1991**, *95*, 4573. (b) Watanabe, M.; Longmire, M. L.; Murray, R. W. *J. Phys. Chem.* **1990**, *94*, 2614. (c) Geng, L.; Reed, R. A.; Longmire, M.; Murray, R. W. *J. Phys. Chem.* **1987**, *91*, 2908.

(12) (a) Lehrer, F. A.; Reiss, H. *J. Appl. Phys.* **1962**, *33*, 2353. (b) Riess, I. *Phys. Rev. B* **1987**, *35*, 5740.

(13) Reiss, H. *J. Phys. Chem.* **1987**, *91*, 5164.

(14) (a) Vorotyntsev, M. A.; Vieil, E.; Heinze, J. *Russ. J. Electrochem.* **1995**, *31*, 1112. (b) Vorotyntsev, M. A. *Synth. Met.* **1993**, *55-57*, 4556. (c) Vorotyntsev, M. A.; Daikhin, L. I.; Levi, M.D. *J. Electroanal. Chem.* **1992**, *332*, 213. (d) Levi, M. D.; Vorotyntsev, M. A.; Kazarinov, V. E. *Synth. Met.* **1991**, *41*, 2923. (e) Kazarinov, V. E.; Levi, M. D.; Skundin, A. M.; Vorotyntsev, M. A. *J. Electroanal. Chem.* **1989**, *271*, 193.

(15) (a) Smith, D.L. *J. Appl. Phys.* **1997**, *81*, 2869. (b) Davis, P. S.; Saxena, A.; Smith, D. L. *J. Appl. Phys.* **1995**, *78*, 4244. (c) Campbell, I. H.; Smith, D. L.; Ferraris, J. P. *Appl. Phys. Lett.* **1995**, *66*, 3030.

(16) (a) Shinar, J. *Synth. Met.* **1996**, *78*, 277. (b) Bronold, F. X.; Saxena, A.; Bishop, A. R. *Phys. Rev. B* **1993**, *48*, 13162.

(17) (a) Reiss, H. *J. Electrochem. Soc.* **1988**, *135*, 247C. (b) Reiss, H. *J. Phys. Chem.* **1985**, *89*, 3783.

(18) Roy Morrison, S. *Electrochemistry at Semiconductor and Oxidized Metal Electrodes*; Plenum Press: New York, 1984; p 46.

(19) Wang, S. *Fundamentals of Semiconductor Theory and Device Physics*; Prentice Hall: Englewood Cliffs, NJ, 1989.

(20) (a) Maness, K.M.; Masui, H.; Wightman, R.M.; Murray, R.W. *J. Am. Chem. Soc.* **1997**, *119*, 1987. (b) Maness, K.M.; Terrill, R.H.; Meyer, T.J.; Murray, R.W.; Wightman, R.M. *J. Am. Chem. Soc.* **1996**, *118*, 10609.

(21) Sum, U.; Fesser, K.; Büttner, H. *Phys. Rev. B* **1989**, *40*, 10509.

(22) Maness, K.M.; Terrill, R.H.; Meyer, T.J.; Murray, R.W.; R.M. Wightman *J. Am. Chem. Soc.* **1996**, *118*, 10609.

(23) (a) Salaneck, W. R.; Brédas, J. L. *Adv. Mater.* **1996**, *8*, 48. (b) Hsieh, B. R.; Ettetgui, E.; Gao, Y. *Synth. Met.* **1996**, *78*, 269.

(24) Planck, M. *Ann. Phys. Chem. N.F.* **1890**, *39*, 161.

(25) (a) Levich, V.G. *Physicochemical Hydrodynamics*; Prentice-Hall: Englewood Cliffs, NJ, 1962; p 249. (b) Sandifer, J. R. In *Ion-Transfer Kinetics*; Sandifer, J. R., Ed.; VCH: New York, 1995; p 123. (c) Mafé, S.; Pellicer, J.; Aguilella, V. M. *J. Phys. Chem.* **1986**, *90*, 6045. (d) McKelvey, J. P. *Solid State Physics for Engineering and Materials Science*; Krieger Publ. Co.: Malabar, FL, 1993; p 424.

(26) (a) MacGillivray, A.D. *J. Chem. Phys.* **1968**, *48*, 2903. (b) Rubinstein, I. *Electrodiffusion of Ions*; SIAM: Philadelphia, 1990; p 107. (c) Mock, M.S. *Analysis of Mathematical Models of Semiconductor Devices*; Boole Press: Dublin, 1983; p 121.